

## Implementation of a Camera-Based Inspection System for Measuring the Diameter of 3D Printed Filaments Made from LDPE Water Bottle Caps

Adhitya Sumardi Sunarya<sup>1</sup>, Wahyu Adhie Candra<sup>1</sup>, Miranti Lestari<sup>1</sup>, Khoutal Taqi<sup>2</sup>,  
Politeknik Manufaktur Bandung, Bandung, Indonesia<sup>1</sup>,  
King Fahd University of Petroleum and Minerals<sup>2</sup>,

**Abstract**— Advances in additive manufacturing technology are driving the need for high-quality, affordable, and sustainable filaments. In Indonesia, the demand for filaments and extruders is largely met through imports, prompting researchers to innovate and develop filament extrusion machines, including those at the Politeknik Manufaktur Bandung, which has developed a filament extrusion machine equipped with a camera-based inspection and control system to produce high-quality filaments from LDPE gallon cap waste. This system integrates a digital microscope camera and a microcontroller to monitor the diameter of the extruded filament and correct the diameter by controlling the speed of the pull motor to stabilize the diameter in real-time. Image processing uses a color-based edge detection algorithm, and camera calibration results show a precision of 0,009 mm/pixel. Diameter data is sent to the Arduino Mega, which then uses the L298N driver to control motor speed via the Sliding Mode Control (SMC) method. Test results show that at 15 RPM, the average filament diameter is 1,77 mm with an error of 1,14%, while at 20 RPM it becomes 1,56 mm with a larger error of 10,86%, compared to the standard commercial filament size of 1,75mm. SMC control also demonstrated better performance than PID in terms of system accuracy in reaching the set point. This system could serve as an economic and ecological solution for local recycled filament production, reducing dependence on imported products.

**Keywords:** diameter, image processing, LDPE, speed control.

Article submitted 2025 July 4.  
Resubmitted 2025 July 10.  
Final acceptance 2025 July 13.  
Final version published as submitted by the authors.

This work is licensed under a [Creative Commons Attribution Share Alike 4.0](https://creativecommons.org/licenses/by-sa/4.0/)



### Corresponding Author:

Miranti Lestari,  
Mechatronics Engineering Technology,  
Politeknik Manufaktur Bandung, Bandung, Indonesia.  
Email: [miranti.lestari@mhs.polman-bandung.ac.id](mailto:miranti.lestari@mhs.polman-bandung.ac.id)

### Citation Document:

Sunarya, A. S., Candra, W. A., Lestari, M., & Taqi, K. (2025). Implementation of a Camera-Based Inspection System for Measuring the Diameter of 3D Printed Filaments Made from LDPE Water Bottle Caps. *Jurnal Edukasi Elektro*, 9(2), 130-148. <https://doi.org/10.21831/jee.v9i2.87996>

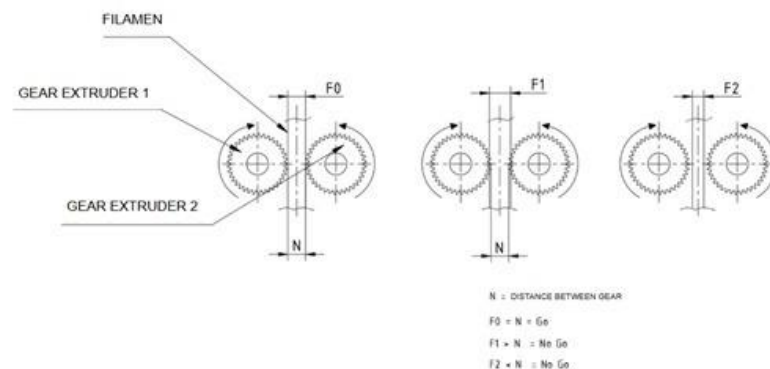
## 1 Introduction

Additive manufacturing technology or better known as 3D printing technology, has become the backbone of the Industrial Revolution 4.0 due to its ability to print complex objects with high precision and efficiency [1],[2],[3]. The increased adoption of this technology has driven the need for

dimensionally stable as high-quality filaments [4]. In Indonesia, most raw materials for 3D printing are still imported, including extruder machines. According to Volza's global market report (2025), Indonesia is listed as one of the top ten importers of extruder machines, with 3,906 shipments from 316 international suppliers during the 2023–2024 period [5].

As a solution, a number of researchers are innovating to create local extruder machines made from plastics waste [6],[7] one of which is the use of raw materials such as LDPE from gallon cap waste has been studied as an alternative filament material. Gallon bottle caps are commonly used in everyday life and are typically discarded after single use, making them a significant contributor to plastic waste[8]. Thermal testing has confirmed that this type of waste exhibits stable melting characteristics and is feasible for extrusion into 3D printing filaments [9]. Muslimin et al. (2024) demonstrated that LDPE based recycled filaments can exhibit functional performance comparable to commercial filaments in terms of shape and tensile strength [1]. However, the main issue in the filament extrusion process is uncontrolled diameter fluctuations. Diameter fluctuations can cause printing defects such as nozzle blockages, poor layer bonding, and dimensional inaccuracies [10],[11],[12].

Figure 1 shows the mechanism of an FDM (Fused Deposition Modeling) or FFF (Fused Filament Fabrication) type 3D printing machine is the most popular additive manufacturing method, in which thermoplastic materials are heated and extruded through a multi-layered nozzle to form 3D objects [13]. Based on the extruder mechanism, there are two extruder gears that push the filament out to print the product. Only filaments with standard dimensions (F0), which are as large as the distance between the gears (N) can be extruded. If the filament is larger in diameter (F1), the extrusion of the filament will cause a jam in the extruder, or if the filament is smaller (F2), it cannot be pulled out for extrusion, and eventually the printing of the product fails.



**Figure 1.** 3D printing extruder mechanism

To address this issue, an automated inspection system based on a camera and digital image processing algorithms offers a promising solution [14],[15]. This system not only detects diameter in real-time [16],[17], but also integrates electronic control to adaptively adjust the speed of the pulling motor. Additionally, speed control based on Sliding Mode Control (SMC) has proven to be more adaptive against system nonlinearity compared to conventional PID methods [18],[19].

This research aims to develop a camera-based digital microscope and image processing system for inspecting the diameter of recycled LDPE filaments, integrated with SMC-based motor speed control using an Arduino Mega microcontroller. The system is expected to maintain filament diameter stability in accordance with commercial standards of 1.75 mm with a tolerance of  $\pm 0.05$  mm [20].

## 2 Method

The method used in this research includes several technical stages. Table 1 shows a list of system demands that must be met in this research as an indicator of research success. Where mechanically

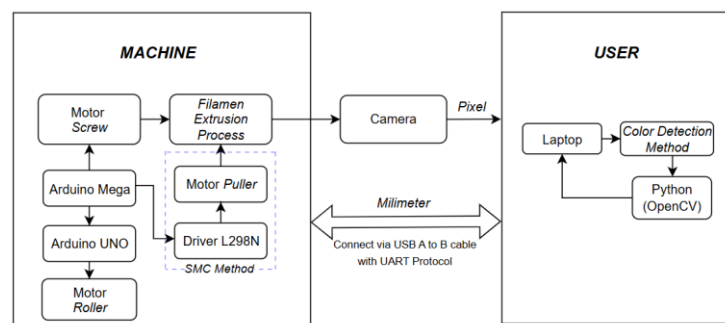
this system must be able to process plastic bottle cap waste into filaments, which is equipped with a visual inspection system. The electrical function must be safe when operated, of course, it must be able to drive the mechanical system according to its function. Then, the designed informatics system algorithm must be able to send the actual diameter measurement results to the microcontroller in real time, so that it can be integrated with a control system that provides control logic to the pulling motor based on signal input from the measurement results by the camera.

**Table 1.** List of system work demands

No.	Domain Tasks	Demands
1	Mechanical System	<ul style="list-style-type: none"> <li>Mechanical System can print 3D printed filaments derived from plastic seeds.</li> <li>Camera-based inspection system does not hinder the extrusion rate.</li> </ul>
2	Electrical System	<ul style="list-style-type: none"> <li>Electrical functions are safe to operate.</li> <li>Capable of effectively driving the mechanical system.</li> </ul>
3	Informatics System	<ul style="list-style-type: none"> <li>Capable of sending control signals to the microcontroller.</li> <li>Capable of measuring filament diameter with an accuracy of less than 0.05 mm..</li> </ul>
4	Control System	<ul style="list-style-type: none"> <li>The system can control the speed of the pulling motor based on filament diameter measurement feedback obtained from the camera.</li> </ul>

Figure 2 shows an overview of the system that is derived from the list of demands that have been defined. The camera acts as an image acquisition device that records the physical shape of the filament produced from the extrusion process. The image data obtained is in the form of filament cross-section, which was originally represented in mm (millimeter) metric units in the camera into pixel units received by a digital image processing device in the form of a laptop. From the user side, image processing algorithms are implemented which include edge detection using the color detection method and utilizing the OpenCV library to convert the pixel scale to mm, then the image acquisition results are transmitted to the towing motor as input for motor speed control. The speed control of the puller motor is programmed with the SMC control method, where the L298N driver which acts as a supply for the motor will receive a signal from the Arduino Mega with the control set as follows.

- If the setpoint > actual diameter, then the speed of the pulling motor is reduced.
- If setpoint < actual diameter, the speed of the puller motor is increased.
- If setpoint = actual diameter, then the speed of the puller motor is constant.

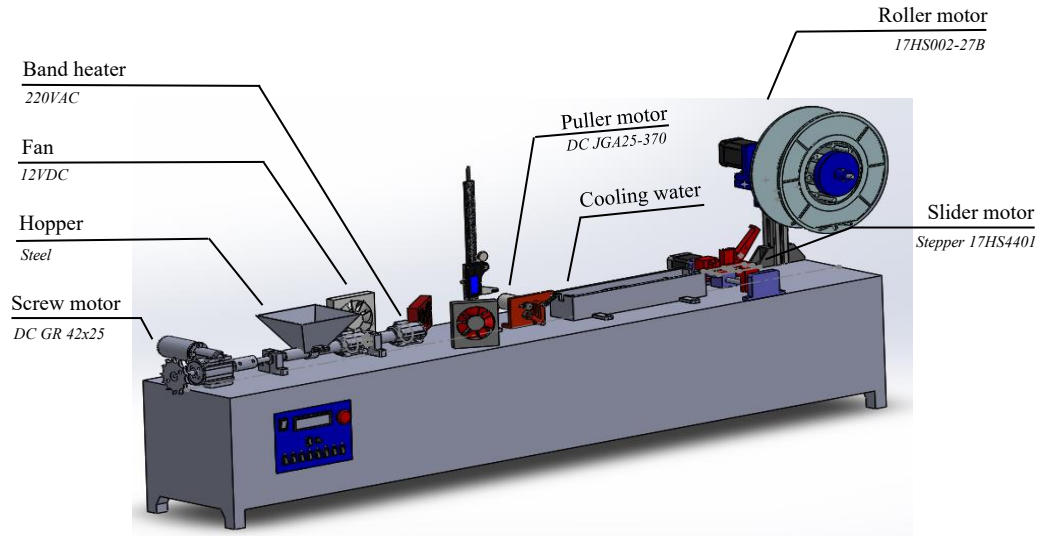


**Figure 2.** System overview

## 2.1 Mechanical system

Figure 3 shows the design of a plastic extruder machine consisting of eight parts: (1) There is the screw motor, which acts as a plastic raw material pusher, (2) There is a hopper, which acts as a temporary container for raw materials, (3) There is a fan, which acts as the first cooling device, (4) There is a band heater that wraps around the extrusion chamber, which acts to melt the raw material so that it can be extruded out of the die, (5) There is a puller motor that pulls the filament as it exits the die, so the puller speed can affect the diameter of the formed filament, (6) There is a water tank

as the second cooling function, (7) There is a slider motor that acts as a filament guide to enter the reel to prevent tangling, (8) There is a roller motor that acts to wind the filament.

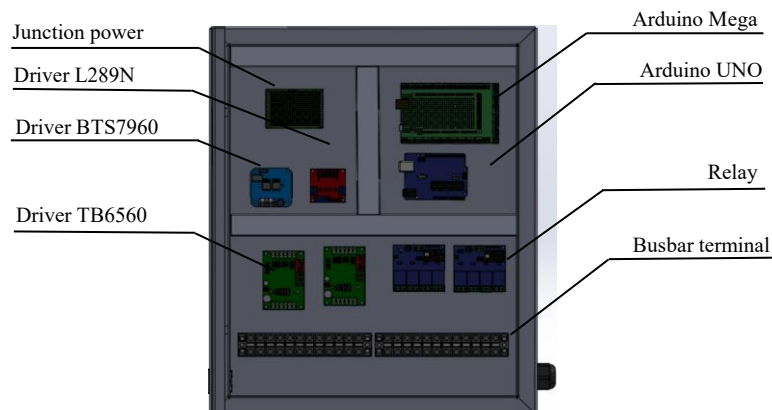


**Figure 3.** Extruder machine design

The machine incorporates two types of motors: DC motors (used for screw and puller motors) and stepper motors (used for slider and roller motors). This selection is strategic, considering the requirements for continuous torque, precise positioning, and efficient control [21],[22]. Where DC motors such as the GR 42×25 and JGA25-370 offer high torque and can be speed regulated using only PWM, they are ideal for maintaining a consistent rate of material being melted through the nozzle. Whereas stepper motors are used in systems that require positional precision, their ability to move in discrete steps without encoders can be used for filament winding systems or filament position adjustment mechanisms.

## 2.2 Electrical system

Figure 4 illustrates the arrangement of components, strategically positioned to ensure safe operation. It shows a power junction acting as a DC voltage source, distributing power to each component according to its specific requirements. Additionally, two types of microcontrollers, two types of DC motor drivers, two types of stepper motor drivers, and two relays are positioned side by side, facilitating ease in cable installation, maintenance, and troubleshooting.



**Figure 4.** Placement of components in panel box

In this electrical system, there are two types of microcontrollers used to build the system architecture in this study. The use of two types of microcontrollers is intended for the needs of task segmentation on the embedded system is necessary to produce an optimized system [23]. The master-slave configuration was chosen because it is effective enough to perform task segmentation where the Arduino Mega serves as the master in charge of receiving the image processing diameter data from the computer, running the motor speed control, and managing the main logic of the system. Meanwhile, the Arduino Uno as a slave is used to handle other actuators that are not included in the main system. This approach is commonly used to share the processing load and expand the flexibility of microcontroller-based systems [24]. Furthermore, the wiring diagram of this master-slave system can be seen in Figure 5.

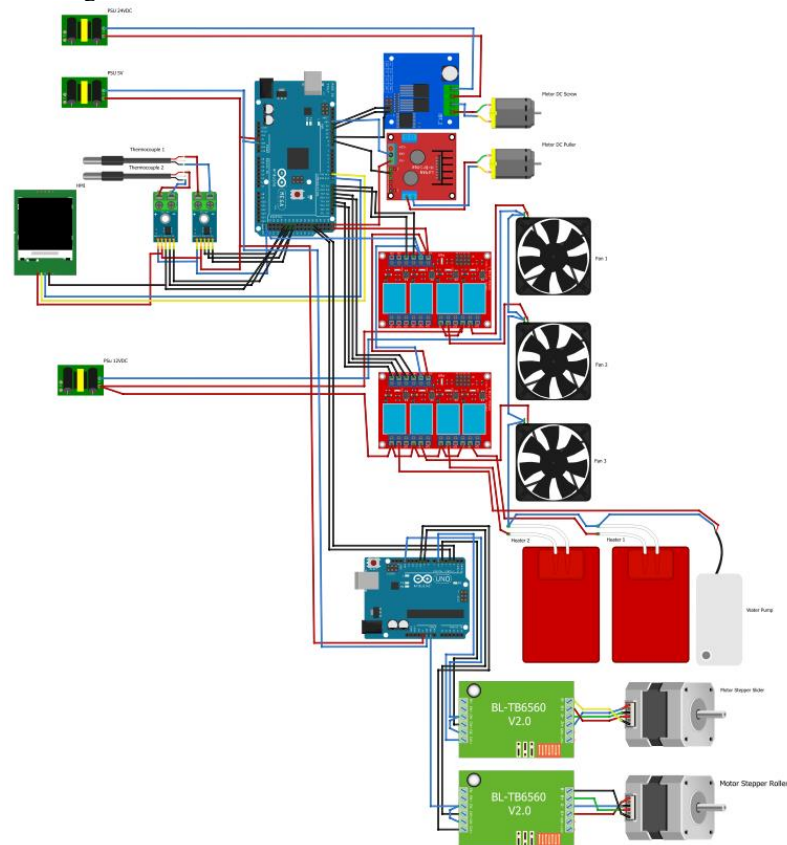
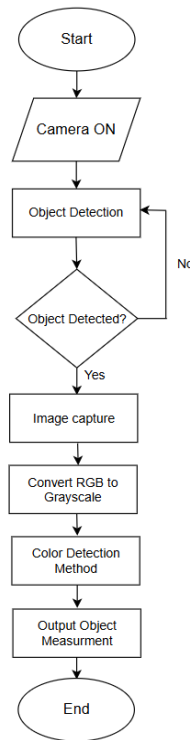


Figure 5. Wiring diagram

### 2.3 Informatics system

Figure 6 shows the information that process starts when the camera is active, then the camera will detect the object. If the object is successfully detected, the camera will capture the image and convert the captured RGB format into grayscale format. Next, a color-based detection method is used to process the captured image for segmentation. This method isolates the target object, in this case the extruded filament, from its background by increasing the visibility of the edges. With a translucent background, the color contrast between the filament and the background is obtained, so the processing algorithm only performs simple color detection, i.e. dark and light, to obtain the edges. This approach is computationally efficient and suitable for microcontroller-based systems, where resources are limited.



**Figure 6.** Image processing flowchart

Previous research has shown that optimized lighting and background configuration significantly improves edge clarity, even in low-complexity embedded systems [25]. After the edge of the object is successfully detected correctly, the diameter of the filament represented in pixel units will be converted into length units in mm [26], so that the output will be obtained in the form of the resulting filament diameter value. To get accurate measurement results, there are three approaches to this calculation process, as follows:

**a) Camera calibration**

The camera calibration in this study was performed using the metric spatial calibration approach, which involves placing a reference object that has a certain physical length represented by one pixel, so that the scale ratio of pixels to millimeters can be calculated accurately [27]. The purpose of this calibration is to determine the actual length represented by one pixel, so that the scale ratio of pixels to millimeters can be calculated accurately. The scale value is obtained through Equation (1), where the physical length of the reference object in millimeters ( $P_{real}$ ) is divided by the number of pixels representing that object in the image ( $P_{px}$ ), resulting in a scale value ( $S_{ref}$ ) in mm/pixel. This value is essential for converting pixel-based measurement results into real length units in the filament diameter measurement process. This calibration process has also been proven to improve measurement accuracy in simple microcontroller-based image processing systems [28].

$$S_{ref} \left( \frac{mm}{px} \right) = \frac{P_{real}}{P_{px}} \quad (1)$$

Explanation:

- $S_{ref}$  : scale ratio (mm/pixel)
- $P_{real}$  : length of physical reference object (mm)
- $P_{px}$  : length of object in image (pixel)

**b) Determine the diameter of the filament**

After the camera calibration process, the filament must be positioned in the same location as the reference object used during calibration to ensure measurement consistency. This method directly applies the scale factor derived from the calibration step to convert the image-based filament width

into the metric unit of length in millimeter. The actual filament diameter ( $D_{real}$ ) is then calculated by multiplying the pixel width of the filament in the image ( $D_{px}$ ) by the scale ratio obtained from Equation 1. Thus, this relationship can be expressed in Equation 2.

$$D_{real} (mm) = D_{px} \times S_{ref} \quad (2)$$

Explanation:

- $D_{real}$  : actual measured filament diameter (mm)
- $D_{px}$  : representation of filament diameter in camera frame (pixel)
- $S_{ref}$  : scale ratio

The camera placement setup is illustrated in Figure 7. As shown, the camera is positioned directly above the filament, with the filament itself placed between the camera and a translucent background. This arrangement ensures clear contrast and optimal lighting conditions, enabling accurate measurement and monitoring of filament diameter during the extrusion process.

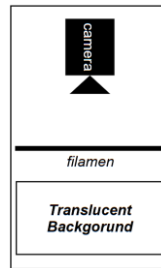


Figure 7. Camera placement scheme (top view)

### c) Average method

To anticipate the shape that is not perfectly straight in the cross section of the measured filament diameter, the average function can be used as an alternative solution to support the success of accurate measurement. It is determined that the ideal filament diameter produced by the extruder machine is 1.75 mm with a tolerance of  $\pm 0.05$  mm. Thus the allowable fluctuation of filament diameter has a lower limit of 1.70 mm while the upper limit is 1.80 mm [20]. Thus,  $f(\text{avg})$  can be expressed as shown in Equation 3.

$$\bar{D} = \frac{\sum_{i=1}^n D_i}{n} \quad (3)$$

Explanation:

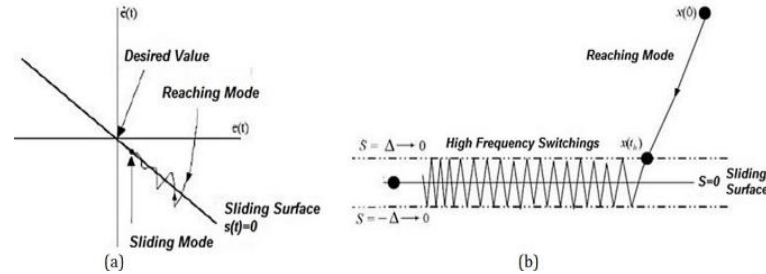
- $\bar{D}$  : average diameter
- $D_i$  : diameter at point –  $i$

## 2.4 Control system

The stability of the filament diameter is affected by the speed of the pulling motor that physically regulates the filament pull, so a control system is needed that can adjust the motor speed accurately based on feedback from sensors in the form of a camera that takes real time measurements of the filament. DC motors that act as puller motors are basically non-linear which has an impact on the efficiency of the controller so that a control is needed. PID (Proportional Integral Derivative) control is widely chosen to regulate the speed of a motor including one of the DC motors. However, if reviewed more deeply, PID control has the disadvantage that it requires a long control design time due to the many parameter settings. Sliding Mode Controller (SMC) control is a non-linear speed controller that is more adaptive [18] by providing speed performance comparable to PID but with better speed performance in terms of overshoot, short settling time [29], and faster system response [19].



The SMC operates by bringing the state of the system to the sliding surface and then to the center point as shown in Figure 8. The sliding surface is the condition where the switching function ( $s$ ) is zero ( $s = 0$ ). The top and bottom are the limiting switching values ( $\pm\Delta$ ). If a state  $x(t) = x(t) > \Delta$  then switching will be off, otherwise if  $x(t) = x(t) \leq \Delta$  then switching will be on [30].



**Figure 8.** (a) Fase SMC (b) Switching mode[30]

The goal of SMC is for the system output to track the desired reference by generating a control signal with minimum error. The control signal in SMC is divided into two, namely reaching mode to bring the system state to the sliding surface which requires switching control ( $u_{sw}$ ) and in the sliding mode state there is an equivalent control ( $u_{eq}$ ) to maintain a stable system state. The sliding mode control (uSMC) signal equation is defined as follows [19].

$$u_{SMC}(t) = u_{eq} + u_{sw} \quad (4)$$

$$u_{sw} = K \cdot \text{sgn}(s) \quad (5)$$

The drawback of SMC is the chattering phenomenon that affects the stability of the control system. Chattering is an oscillation phenomenon with a high frequency occurring at the control input. Pseudo sliding can be used to reduce chattering with smooth control action.

$$u_{sw} = K_s \cdot \frac{s}{|s| + \delta} \quad (6)$$

Where  $\delta$  is a small tuning scalar referred to as the tuning parameter to reduce chattering [19].

Based on empirical data obtained through testing speed variation (rpm) on the diameter of the filament produced, a linear regression was performed to obtain a model of the input-output relationship [31],[32]. The regression results provide a simple linear model as follows.

$$d = m \cdot \text{rpm} + c \quad (7)$$

Furthermore, this linear model is used to form the first-order plant transfer function model:

$$G(s) = \frac{D(s)}{V(s)} = \frac{K}{\tau s + 1} \quad (8)$$

Explanation:

$D(s)$  : system output which is the filament diameter in Laplace domain.

$V(s)$  : system input in the form of puller motor speed.

$K = m$  : is the plant gain, with invers relation.

$\tau$  : is the plant time constant, estimated based on experimental results of physical system.

rpm : puller motor speed

Thus, the equation in the time domain equivalent to this model can be written as:

$$\tau \dot{D}(t) + D(t) = K v(t) \quad (9)$$

Explanation:

$D(t)$  : actual diameter in time domain

$v(t)$  : puller motor speed control signal in time domain



In designing SMC control, this control works by defining a sliding surface (s) to steer the system towards the equilibrium point. The value (s) in this study can be defined from the error  $e$  and its derivative ( $\dot{e}$ ):

$$s = c \cdot e + \dot{e} \quad (10)$$

The value of ( $e$ ) is the difference in error from:

$$e = D_s - D_a \quad (11)$$

Then the sliding surface (s) is obtained:

$$s = c \cdot (D_s - D_a) + \frac{d}{dt}(D_s - D_a) \quad (12)$$

Explanation:

$c > 0$  : is a design parameter that regulates the rate of error convergence

$D_s$  : setpoint diameter

$D_a$  : actual diameter

SMC control has the characteristic of forcing the system to go to and maintain a state on the sliding surface  $s = 0$ , so that the error ( $e$ ) can converge to zero quickly and stably.

$$s = 0 \Rightarrow \dot{s} = 0$$

Based on equation (10), it is obtained:

$$s = c \cdot e + \dot{e} = 0$$

$$\dot{e} = -c \cdot e \quad (13)$$

Considering equation (11), under the condition that  $D_s$  is constant, the error derivative can be subsumed into:

$$\dot{e} = -\dot{D}_a = -c \cdot e = -c(D_s - D_a) \quad (14)$$

Thus,

$$\dot{D}_a = c(D_s - D_a) \quad (15)$$

Substitute equation (15) into the linear plant model equation in (9), thus the equivalent control ( $u_{eq}$ ) is obtained:

$$\tau c(D_s - D_a) + D_a = Kv \quad (16)$$

The equivalent control is the motor speed signal required to keep the system on the sliding surface. Thus, the final SMC signal control equation (uSMC) is in equation (17):

$$u_{SMC} = \frac{1}{K} (\tau c(D_s - D_a) + D_a) + K_s \cdot \frac{c \cdot e + \dot{e}}{|c \cdot e + \dot{e}| + \delta} \quad (17)$$

Explanation:

$K_s > 0$  : is a switching gain parameter

$\delta > 0$  : is a parameter that smooths the saturation to reduce the chattering effect

Thus, a closed control system block diagram is obtained as shown in Figure 9, where the filament diameter is the system input which then there is system control with the smc control method to control the speed of the puller motor so as to produce a filament diameter according to the setpoint, the measurement from the camera is used as system feedback to provide an error signal.

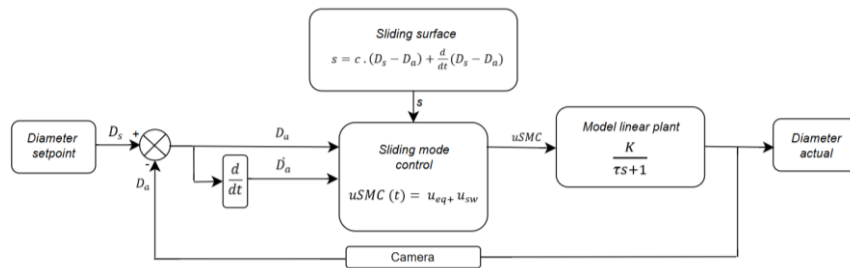


Figure 9. Block diagram of control system

### 3 Result

#### 3.1 Hardware implementation

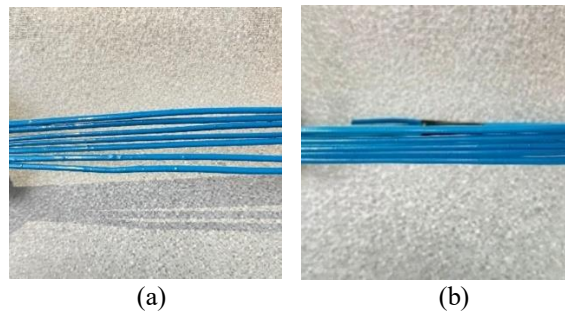
Figure 10 presents a complete view of the horizontal extrusion system that integrates all essential stages in filament production from material input to spooling. Starting from the left, (1) the screw motor serves as the driving force to rotate the extrusion screw, while (2) the hopper is used to insert LDPE plastic pellets as raw material. These pellets are then heated by (3) the band heater and pushed forward through the barrel.

The molten plastic is propelled toward the outlet and passes through (4) dual cooling fans, which help solidify the extruded filament. In the center of the system, (5) a digital microscope camera is mounted directly above the filament path to monitor its diameter in real time. The camera is supported by a translucent background and even lighting to enhance edge detection accuracy during image processing. Next, (6) the puller motor maintains a constant tension and pulling speed, ensuring consistent diameter output. To stabilize thermal conditions, (7) a cooling water pump system is placed under the filament path. The extruded filament is then collected using (8) a slider motor and finally rolled onto a spool using (9) a roller motor, which ensures tidy and aligned winding.



Figure 10. Extruder machine implementation

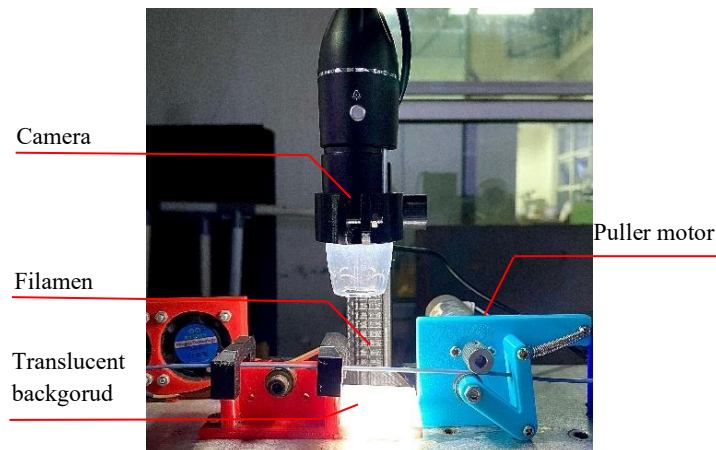
The operating temperature of this extrusion machine is relatively low, running in the range of 105-115°C which corresponds to the melting point of LDPE plastic [33], [34] with the raw materials having to be shredded first. The finer the shredding, the finer and more uniform the filaments produced. As illustrated in Figure 11, the quality of the shredding process significantly affects the filament yield where (a) coarse grains produce lumpy and irregular filaments due to melting consistency and insufficient flow during extrusion, whereas (b) shows that fine grains allow for better processing, resulting in smoother and more consistent filaments.



**Figure 11.** (a) Coarse chopping, (b) fine chopping

Figure 12 is an implementation of the design in Figure 7, where the digital microscope camera is placed in top-view, parallel to the extruded filament trajectory. To improve edge contrast and reduce noise in the captured images, a translucent background is used under the filament made of 12VDC LEDs, and the lighting source from the built-in digital camera is used. This configuration supports successful edge detection using a color-based segmentation algorithm, making the measurement more stable and accurate.

The detected filament diameter will be processed in real-time and sent as feedback to the Arduino Mega which acts as the main controller. Based on the difference to the setpoint of 1.75 mm, the microcontroller will send a control signal to adjust the speed of the puller motor through the L298N driver. This closed loop mechanism ensures that the filament remains within the diameter tolerance during the extrusion process.



**Figure 12.** Camera placement implementation

### 3.2 Interface

Figure 13 shows the GUI system developed in this study features a live top-view camera feed that captures the extruded filament in real time. The image display is enhanced using a translucent background and backlighting to increase edge contrast. A color-based edge detection algorithm is applied, resulting in yellow contour lines that delineate the filament's left and right edges. This visual cue not only facilitates precise diameter measurement in millimeters but also reflects the effectiveness of the implemented image processing method for real-time monitoring.

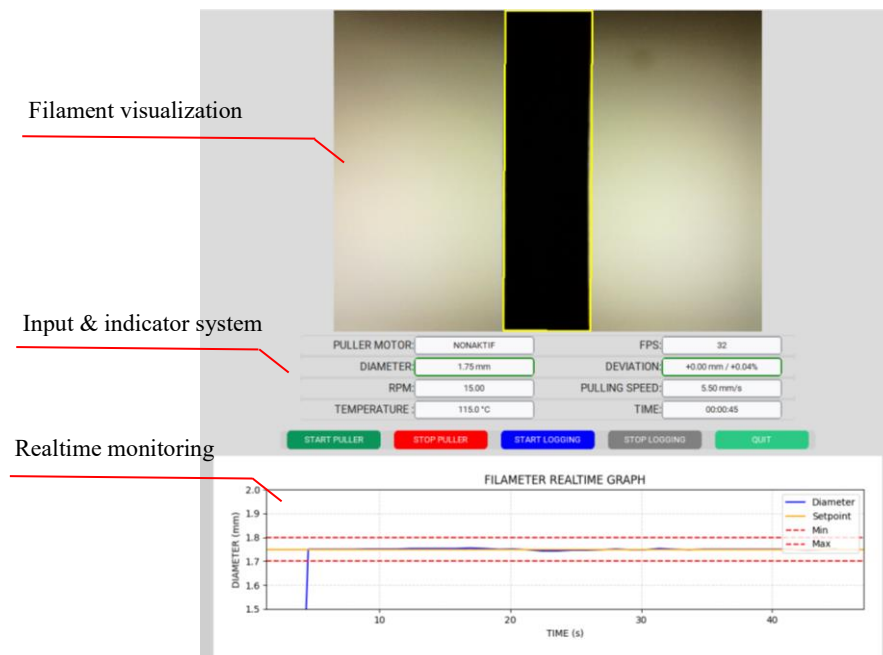


Figure 13. Interface

### 3.3 Device testing

In image-based measurement systems, camera calibration is a critical step to ensure the accuracy of dimensional analysis. The calibration process establishes the scale ratio between pixel units and actual physical dimensions, which is essential when the measurement system is used for real-time control and feedback [26], [27].

This test aims to validate the accuracy of the digital microscope camera used in the extrusion monitoring system. Before conducting diameter measurements, a metric calibration was performed using a block gauge with a certified physical dimension of 1.5 mm. The block gauge was selected due to its widespread use in standard calibration and its high precision in dimensional reference. Calibration was performed at a fixed working distance of 5.5 cm using a manufacturer-designed calibration ruler, which allowed direct measurement in pixel units. Based on Equation 1, the scale factor is determined as:

$$S_{ref} = \frac{4\text{mm}}{426\text{px}} = 0.009 \text{ mm/px}$$

To evaluate accuracy, the camera was used to measure the same block gauge 20 times. Table 2 shows that most errors were within  $\pm 0.2\%$ , with an average error of just 0.041%, demonstrating a very high degree of measurement reliability. These results confirm that the system is capable of measuring filament diameter with an accuracy better than  $\pm 0.05 \text{ mm}$ , as required for maintaining 3D printing filament standards.

Table 2. Camera calibration test results

Test	Test piece (mm)	Camera Testing (mm)	Error (%)
1		1.4987	0.087
2		1.5025	0.167
3		1.5000	0.000
4		1.5000	0.000
5		1.5029	0.193


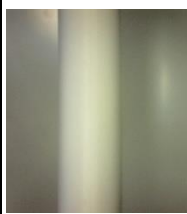

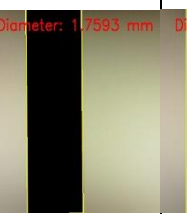



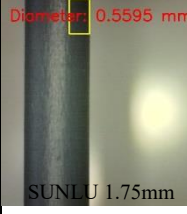


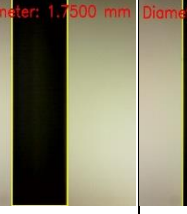

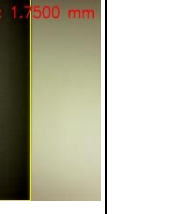
Test	Test piece (mm)	Camera Testing (mm)	Error (%)
6	 (Block gauge)	1.4992	0.053
7		1.5000	0.000
8		1.5016	0.107
9		1.5000	0.000
10		1.5020	0.133
11		1.5000	0.000
12		1.5000	0.000
13		1.5000	0.000
14		1.5000	0.000
15		1.4990	0.067
16		1.5002	0.013
17		1.5000	0.000
18		1.5000	0.000
19		1.5000	0.000
20		1.5000	0.000
Mean error (%)			0.041

Figure 14 shows that testing the measurement accuracy on a 1.75 mm commercial filament with a tolerance of  $\pm 0.05$  mm at various lighting levels has a direct effect on the quality of edge segmentation and the accuracy of computer vision-based filament diameter measurement [33],[34]. Under ambient lighting conditions, measured at 220 lux, the eSUN filament cannot be recognized as having a color close to the background. In contrast, SUNLU filaments are still partially recognizable, even though their edge contours are not segmented.

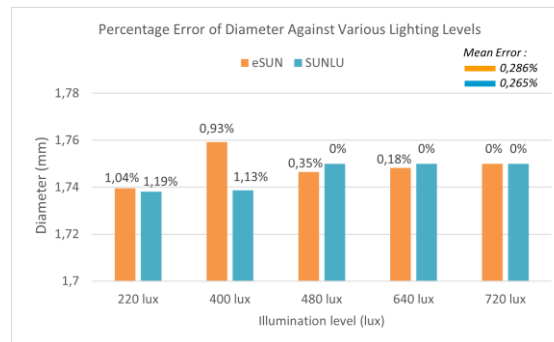
As the illumination level increases from 400-720 lux, the segmentation quality improves significantly, as shown by the more accurate edge detection that results in diameter measurement values that have 0% error with the actual object. This shows that controlled illumination is an important requirement in image-based inspection systems to avoid detection failures due to low contrast between the object and the background. The simple solution of using a translucent background also provides reliable measurement results.

Original	Level 0 (220 lux in ambience)	Level 1 (400 lux)	Level 2 (480 lux)	Level 3 (640 lux)	Level 4 (720 lux)
					
eSUN 1.75mm	Diameter: 1.7398 mm	Diameter: 1.7593 mm	Diameter: 1.7485 mm	Diameter: 1.7482 mm	Diameter: 1.7500 mm
					
SUNLU 1.75mm	Diameter: 0.5595 mm	Diameter: 1.7381 mm	Diameter: 1.7387 mm	Diameter: 1.7500 mm	Diameter: 1.7500 mm

**Figure 14.** Commercial filament measurement results

Figure 15 shows that the error of the filament diameter measurement decreases significantly as the lighting intensity increases from 220 lux to 720 lux. Both filament types (eSUN and SUNLU) experience a decrease in error, but SUNLU shows a more stable and accurate measurement performance, as evidenced by the error reaching 0% from 480 lux to 720 lux, with an average error of 0.265%, better than eSUN which reaches 0.286%.

This difference is closely related to the visual characteristics of filament color and the way the system detects edges using color-based methods through color thresholding and contour extraction procedures. The white eSUN filaments tend to have low contrast against the translucent background, especially at low light intensity. This causes difficulty in edge segmentation as the object boundaries become less defined. In contrast, SUNLU filaments, which tend to be darker, provide higher contrast, making it easier for the system to extract object contours, resulting in more consistent diameter measurements [33], [34].



**Figure 15.** Percentage error of diameter against various lighting levels

### 3.4 System testing

System testing is carried out in three stages, the first stage is to get an overview of the relationship between speed and diameter, the second stage is to find the speed value that will be used as a system reference (base rpm) to get filaments that match the setpoint, and the third stage will be testing a system that has been integrated between camera measurements and motor speed control using PID and SMC controls to get more optimal control in terms of producing more consistent filaments.

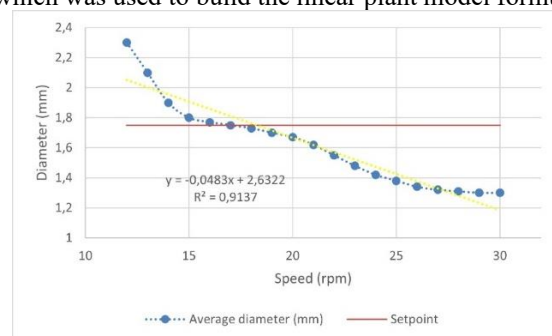
Table 3 shows that the puller motor can rotate at a minimum speed of 12 rpm and produce filaments with an average diameter of 2.3 mm with the maximum speed limited to 30 rpm only because it has passed the moment of the lower limit value of the filament diameter of 1.7 mm. It was found that to obtain a diameter value that complies with the standard of 1.75 mm with a tolerance of <0.05 mm, the upper limit of the allowable diameter is 1.8 mm and the lower limit is 1.7 mm at speeds of 15 rpm and 20 rpm, so further validation testing is carried out to determine the reference speed that produces filaments with a diameter close to the setpoint.

**Table 3.** First test results

Speed (rpm)	Setpoint (mm)	Average output diameter (mm)	Error (%)
12	1.75	2.30	31.43
13		2.10	20.00
14		1.90	8.57
15		1.80	2.86
16		1.77	1.14
17		1.73	1.14
18		1.71	2.29
19		1.70	2.86
20		1.67	4.57
21		1.62	7.43
22		1.55	11.43
23		1.48	15.43

Speed (rpm)	Setpoint (mm)	Average output diameter (mm)	Error (%)
24		1.42	18.86
25		1.38	21.14
26		1.34	23.43
27		1.34	23.43
28		1.32	24.57
29		1.31	25.14
30		1.30	25.71
Mean error (%)			14.29

Figure 16 shows the characteristic relationship of the system where the test results show that (v) the speed of the puller motor, which plays a role in pulling the filament, produces an inverse relationship to (d) the diameter of the filament produced, where the diameter of the filament decreases linearly as the speed of the puller motor increases. Thus, a linear regression equation  $y = -0.0483x + 2.6322$  was obtained which was used to build the linear plant model formulated in Equation 7.



**Figure 16.** Relation between speed and diameter

Table 4 shows the results of validation testing at 15 rpm and 20 rpm to find the reference speed and set as the base speed of the system to produce filaments in accordance with the setpoint. It was found that, at a speed of 15 rpm produces an average filament diameter of 1,77 mm with an error from the setpoint diameter of 3,66%, while at a speed of 20 rpm produces an average filament diameter of 1,56 mm with an error from the setpoint reaching 10,86%. Therefore, it can be stated that the 15-rpm speed produces a filament distribution consistency that is closer to the setpoint than the 20-rpm speed. Thus, this 15-rpm speed will be used as the reference speed (base speed) to compare PID control and SMC control to produce consistent filaments within the allowed diameter range.

**Table 4.** Validation testing

Point	Setpoint (mm)	Average diameter at 15 rpm	Average diameter at 20 rpm
1	1.75	1.79	1.75
2		1.75	1.66
3		1.89	1.47
4		1.83	1.36
5		1.84	1.39
6		1.79	1.58
7		1.79	1.57
8		1.7	1.61
9		1.76	1.63
10		1.58	1.58
Average (mm)		1.77	1.56
Mean Error (%)		3.66	10.86

To further evaluate the effectiveness of the control system in maintaining filament diameter consistency, comparative testing was conducted between the PID and SMC at a selected base speed of



15 rpm, the base speed of 15 rpm was selected based on the test validation results in Table 7 showing that at 15 rpm there is a higher potential to produce filaments close to the setpoint value. At this stage, both control strategies were tested at thirty different measurement points to assess their ability to keep the filament diameter within the commercial tolerance range of  $\pm 0.05$  mm. Each point was analyzed against the commercial tolerance limits of  $\pm 0.05$  mm (upper limit of 1.80 mm and lower limit of 1.70 mm). This test model adopts the approach taken by Noor et al. (2024), who also evaluated diameter consistency with point measurements on filament samples to determine the optimal parameters[20]. This study adapted the same principle to evaluate the control performance quantitatively.

Figure 17 shows that PID control results in larger diameter fluctuations, with the distribution of values mostly occurring at points that exceed the tolerance limit, where the mean system error reaches 4.65% against the diameter setpoint. In contrast, the SMC showed better stability, keeping the diameter within the tolerance limits with a mean system error of only 1.87%. These findings confirm that SMC is more reliable and adaptive in handling systems that require fast error correction.

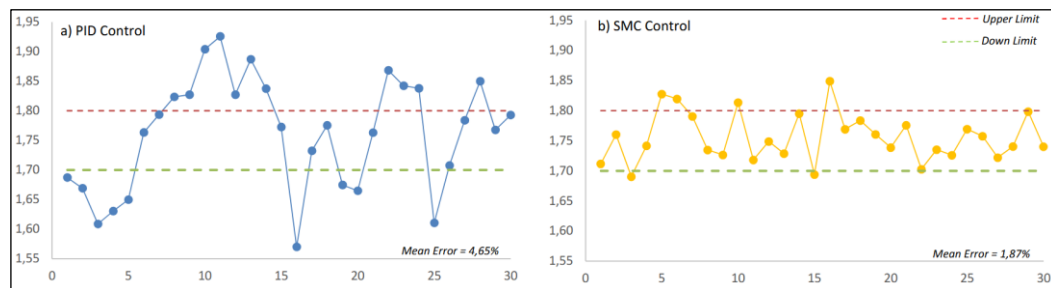


Figure 17. Diameter consistency for PID and SMC method

## 4 Discussion

This research focuses on the development of a digital camera-based inspection system integrated with a motor speed control system to maintain the stability of the filament diameter resulting from the extrusion process. The main objective of the system is to create a closed-loop control based on real-time visual reading that can correct the diameter directly through the speed regulation of the puller motor. The developed system successfully realized closed-loop control between diameter detection and puller motor speed. The test results show that the system can measure the diameter with high accuracy, store the data, and adjust the motor speed automatically based on the deviation from the diameter setpoint. The implemented controller provides adaptive responses showing fast correction capability to the fluctuation of filament diameter.

This research does not explicitly address control stability analysis in the context of dynamic system control. The test methodology was designed in a structured manner to prioritize the achievement of output diameter stability, through the stages of: (1) analysis of extrusion system characteristics, (2) selection of the base speed to obtain the potential stability of the resulting diameter, thus limited speed testing, and (3) comparison of PID and SMC controller performance in terms of adaptivity to measurement error correction converted into speed control. The emphasis on the adaptive aspect is based on the need for the system to respond quickly to changes in diameter, rather than being adaptive to persistent disturbances. Future research can focus on analyzing the stability of the control system and the diameter detection method can also be enhanced with a machine learning-based approach to improve accuracy under varied environmental conditions that are not accommodated by the methods that have been implemented in this system.

## 5 Conclusion

This research successfully developed a filament extrusion system that integrates a real-time camera-based inspection system using color-based edge detection and OpenCV. This method shows measurement results with accuracy reaching 0.009 mm/pixel with a detection accuracy rate of 99.959%, where the error margin is only 0.041%. Testing the measurement accuracy in the illumination range of 220-720 lux shows that the optimal illumination is  $\geq 480$  lux which significantly improves the segmentation accuracy with an mean error ranging from 0.265% - 0.286%. The high contrast between the filament and the background ensures better edge segmentation, thus improving the reliability of real-time measurement.

In addition, the system test results show that the draw speed at 15 RPM is more effective in achieving the target diameter of 1.75 mm with a deviation of 3.66%. The application of Sliding Mode Control (SMC) control further enhances the system's ability to maintain filament diameter consistently and is more adaptive when compared to PID control. Overall, the developed system offers an economically and ecologically promising solution to produce high-quality recycled LDPE filaments locally, reducing dependence on imported products and contributing to sustainable additive manufacturing practices in Indonesia.

## 6 References

- [1] Muslimin *et al.*, 'Utilization of Recycle LDPE (r-LDPE) Plastic and Galangal Stem Fiber for the Development of 3D Printing Filaments', *Mater. Sci. Forum*, vol. Vol. 1134, pp.125–134, Dec. 2024, doi: 10.4028/p-sf9nRH.
- [2] D. Dubey, S. P. Singh, and B. K. Behera, 'A review on recent advancements in additive manufacturing techniques', *Proc. Inst. Mech. Eng. Part E J. Process Mech. Eng.*, p. 09544089241275860, Aug. 2024, doi: 10.1177/09544089241275860.
- [3] '3D printing and International Trade: What is the evidence to date?', OECD Trade Policy Papers 256, Nov. 2021. doi: 10.1787/0de14497-en.
- [4] K. Yu, Q. Gao, L. Lu, and P. Zhang, 'A Process Parameter Design Method for Improving the Filament Diameter Accuracy of Extrusion 3D Printing', *Materials*, vol. 15, no. 7, p. 2454, Mar. 2022, doi: 10.3390/ma15072454.
- [5] 'Extruder Machine Buyers & Importers in Indonesia - Volza'. Accessed: Jun. 18, 2025. [Online]. Available: <https://www.volza.com/ogimages/buyers/e/extruder-machine-buyers-in-indonesia-buyers.svg>
- [6] M. L. Sonjaya, M. Mutmainnah, and M. F. Hidayat, 'Construction of Plastic Waste Extruding Machine to Produce Filaments of 3D Printing Machine', *Int. J. Mech.*, vol. 16, pp. 82–90, Jul. 2022, doi: 10.46300/9104.2022.16.10.
- [7] Y. K. P. Saleh, M. Zaenudin, M. M. Al Azzam, A. K. Bakar, and A. N. Haryudiniarti, 'Filament maker design for Polyethylene Terephthalate(PET) plastic bottle recycling', presented at the 2ND INTERNATIONAL CONFERENCE SERIES ON SCIENCE, ENGINEERING, AND TECHNOLOGY (ICSSET) 2022, Sidoarjo, Indonesia, 2024, p. 060009. doi: 10.1063/5.0218078.
- [8] P. G. C. Nayanathara Thathsarani Pilapitiya and A. S. Ratnayake, 'The world of plastic waste: A review', *Clean. Mater.*, vol. 11, p. 100220, Mar. 2024, doi: 10.1016/j.clema.2024.100220.
- [9] M. Apriliani, 'THERMAL TEST OF 3D PRINTING FILAMENTS FROM PLASTIC WASTE AS AN ENVIRONMENTALLY FRIENDLY PRINTING MEDIA ALTERNATIVE', *Kreator*, vol. 10, no. 2, pp. 36–39, Feb. 2024, doi: 10.46961/kreator.v10i2.876.
- [10] D. P. Da Silva *et al.*, 'Property mapping of LDPE during 3D printing: evaluating morphological development with X-ray scattering', *Front. Mech. Eng.*, vol. 9, p. 1232562, Aug. 2023, doi: 10.3389/fmech.2023.1232562.
- [11] Sr Vehicle Integration Engineer, USA, S. Naveen D Surabhi, M. Dolu Surabhi, and Quality Assurance Engineer, USA, 'Enhancing Dimensional Accuracy in Fused Filament Fabrication: A DOE Approach', *J. Mater. Sci. Manuf. Res.*, pp. 1–7, Apr. 2024, doi: 10.47363/JMSMR/2024(5)177.

- [12] F. Tikhani and P. Hubert, 'Extrusion optimization and advanced mechanical characterization of fibre-reinforced polycarbonate filaments: Improving performance for fused filament fabrication', *Compos. Part Appl. Sci. Manuf.*, vol. 191, p. 108752, Apr. 2025, doi: 10.1016/j.compositesa.2025.108752.
- [13] R. B. Kristiawan, F. Imaduddin, D. Ariawan, Ubaidillah, and Z. Arifin, 'A review on the fused deposition modeling (FDM) 3D printing: Filament processing, materials, and printing parameters', *Open Eng.*, vol. 11, no. 1, pp. 639–649, Apr. 2021, doi: 10.1515/eng-2021-0063.
- [14] R. Badarinath and V. Prabhu, 'Real-Time Sensing of Output Polymer Flow Temperature and Volumetric Flowrate in Fused Filament Fabrication Process', *Materials*, vol. 15, no. 2, p. 618, Jan. 2022, doi: 10.3390/ma15020618.
- [15] K. T. Werkle, C. Trage, J. Wolf, and H.-C. Möhring, 'Generalizable process monitoring for FFF 3D printing with machine vision', *Prod. Eng.*, vol. 18, no. 3–4, pp. 593–601, Jun. 2024, doi: 10.1007/s11740-023-01234-2.
- [16] R. Zende and R. Pawade, 'A novel IoT based machine vision system for on-machine diameter measurement and optimization', *Eng. Res. Express*, vol. 5, no. 4, p. 045075, Dec. 2023, doi: 10.1088/2631-8695/ad0c8c.
- [17] B. M U, H. Raghuram, and Mohana, 'Real Time Object Distance and Dimension Measurement using Deep Learning and OpenCV', in *2023 Third International Conference on Artificial Intelligence and Smart Energy (ICAIS)*, Coimbatore, India: IEEE, Feb. 2023, pp. 929–932. doi: 10.1109/ICAIS56108.2023.10073888.
- [18] A. M. Almawla, M. J. Hussein, and A. T. Abdullah, 'A Comparative Study of DC Motor Speed Control Techniques Using Fuzzy, SMC and PID', *J. Eur. Systèmes Autom.*, vol. 57, no. 2, pp. 397–406, Apr. 2024, doi: 10.18280/jesa.570209.
- [19] H. Maghfiroh, A. Sujono, M. Ahmad, and C. H. B. Apribowo, 'Basic Tutorial on Sliding Mode Control in Speed Control of DC-motor', *J. Electr. Electron. Inf. Commun. Technol.*, vol. 2, no. 1, Apr. 2020, doi: 10.20961/jeeict.2.1.41354.
- [20] H. Mohammad Noor, M. Ibrahim, A. A. A. Norazaman, D. Abu Bakar Sidik, R. Mohd Adnan, and N. S. Mohd Aripin, 'Parameter Optimization in FDM Filament Fabrication via Single Screw Extruder', *PaperASIA*, vol. 40, no. 4b, pp. 266–272, Aug. 2024, doi: 10.59953/paperasia.v40i4b.203.
- [21] M. H. Wankhade and S. G. Bahale, 'Design and Development of Plastic Filament Extruder for 3D Printing', *IRA-Int. J. Technol. Eng. ISSN 2455-4480*, vol. 10, no. 3, p. 23, May 2018, doi: 10.21013/jte.v10.n3.p1.
- [22] M. El Mrabet, Z. Mekrini, A. El Mesbahi, and M. Boulaala, 'Comparative simulation study of electric motors for high performance of 3D printers', *TELKOMNIKA Telecommun. Comput. Electron. Control*, vol. 21, no. 4, p. 935, Aug. 2023, doi: 10.12928/telkomnika.v21i4.24210.
- [23] W. Fabre, K. Haroun, V. Lorrain, M. Lepecq, and G. Sicard, 'From Near-Sensor to In-Sensor: A State-of-the-Art Review of Embedded AI Vision Systems', *Sensors*, vol. 24, no. 16, p. 5446, Aug. 2024, doi: 10.3390/s24165446.
- [24] 'Optimizing Master-Slave Communication in Collaborative Robotics Using IoT-Enabled Robot Interaction', *Indian J. Pure Appl. Phys.*, 2024, doi: 10.56042/ijpap.v62i11.12403.
- [25] Z. Feng, R. Shi, Y. Jiang, Y. Han, Z. Ma, and Y. Ren, 'A Multiscale Gradient Fusion Method for Color Image Edge Detection Using CBM3D Filtering', *Sensors*, vol. 25, no. 7, p. 2031, Mar. 2025, doi: 10.3390/s25072031.
- [26] 'Object size measurement and camera distance evaluation for electronic components using Fixed-Position camera', *Comput. Vis. Stud.*, 2023, doi: 10.58396/cvs020101.
- [27] Y. Tu *et al.*, 'Dimensional Accuracy Evaluation of Single-Layer Prints in Direct Ink Writing Based on Machine Vision', *Sensors*, vol. 25, no. 8, p. 2543, Apr. 2025, doi: 10.3390/s25082543.
- [28] M. F. Khan, E. M. A. Dannoun, M. M. Nofal, and M. Mursaleen, 'Significance of Camera Pixel Error in the Calibration Process of a Robotic Vision System', *Appl. Sci.*, vol. 12, no. 13, p. 6406, Jun. 2022, doi: 10.3390/app12136406.
- [29] J. W. Chan, 'Sliding Mode Control of Brushless DC Motor Speed Control', *Malays. J. Sci. Adv. Technol.*, pp. 188–193, Oct. 2022, doi: 10.56532/mjsat.v2i4.57.
- [30] E. H. Dursun and A. Durdu, 'Speed Control of a DC Motor with Variable Load Using Sliding Mode Control', *Int. J. Comput. Electr. Eng.*, 2016, doi: 10.17706/ijcee.2020.8.3.219-226.

- [31] K.-E. Min, J.-W. Jang, J. Shin, C. Kim, and S. Yi, 'Development of Prediction Method for Dimensional Stability of 3D-Printed Objects', *Appl. Sci.*, vol. 13, no. 19, p. 11027, Oct. 2023, doi: 10.3390/app131911027.
- [32] P. Minetola and A. Giubilini, 'A preliminary study on multi-material fused filament fabrication of an embedded strain gauge for low-cost real-time monitoring of part strain', *Prog. Addit. Manuf.*, vol. 9, no. 6, pp. 2273–2290, Dec. 2024, doi: 10.1007/s40964-024-00582-4.
- [33] C. Hu, B. B. Sapkota, J. A. Thomasson, and M. V. Bagavathiannan, 'Influence of Image Quality and Light Consistency on the Performance of Convolutional Neural Networks for Weed Mapping', *Remote Sens.*, vol. 13, no. 11, p. 2140, May 2021, doi: 10.3390/rs13112140.
- [34] T. Wang, G.-T. Kim, J. Shin, and S.-W. Jang, 'Hierarchical Image Quality Improvement Based on Illumination, Resolution, and Noise Factors for Improving Object Detection', *Electronics*, vol. 13, no. 22, p. 4438, Nov. 2024, doi: 10.3390/electronics13224438.

## 7 Authors Biography

**Adhitya Sumardi Sunarya** is a senior lecturer at the Department of Mechatronics Engineering, Politeknik Manufaktur Bandung. His research focuses on applied physics, control systems, and digital measurement systems. He has published several works indexed in national and international journals, including in IOP Conference Series and IEEE. His projects often involve real-time systems, embedded microcontrollers, and sensor-based automation (email: adhitya@ae.polman-bandung.ac.id).

**Wahyu Adhie Candra** is a lecturer and researcher at the Department of Aerial System Engineering Technology, Politeknik Manufaktur Bandung. His expertise includes robotics, embedded systems, instrumentation, and automation in vocational and industrial applications. He has co-authored research on mobile robot systems, QR-code-based inventory management, and smart library automation. His research contributions are listed in RESTI Journal, Jurnal Vokasi, and other peer-reviewed platforms (email: wahyu@polman-bandung.ac.id).

**Miranti Lestari** is an undergraduate student at Bandung Polytechnic for Manufacturing in the Applied Bachelor Program of Mechatronics Engineering Technology. Her research interests include embedded systems, image processing, control systems, and sustainable development for additive manufacturing technologies. She actively contributes to department-led research projects in the field of mechatronics (email: miranti.lestari@mhs.polman-bandung.ac.id).

**Khoutal Taqi** is a student of Electrical Engineering at King Fahd University of Petroleum and Minerals (KFUPM), Saudi Arabia. His academic interests include power systems, control engineering, and embedded electronics. He is currently involved in undergraduate research and engineering development projects (email: g202304210@kfupm.edu.sa).